Steel and Composite Structures, *Vol. 24, No. 5 (2017) 579-589*
DOI: https://doi.org/10.12989/scs.2017.24.5.579

Post-buckling responses of functionally graded beams with porosities

Şeref D. Akbaş*

Department of Civil Engineering, Bursa Technical University, Yıldırım Campus, Yıldırım, Bursa 16330, Turkey

(*Received February 16, 2017, Revised April 11, 2017, Accepted May 16, 2017*)

Abstract. The objective of this work is to analyze post-buckling of functionally graded (FG) beams with porosity effect under compression load. Material properties of the beam change in the thickness direction according to power-law distributions with different porosity models. It is known that post-buckling problems are geometrically nonlinear problems. In the nonlinear kinematic model of the beam, total Lagrangian finite element model of two dimensional (2-D) continuum is used in conjunction with the Newton-Raphson method. In the study, the effects of material distribution, porosity parameters, compression loads on the post-buckling behavior of FG beams are investigated and discussed with porosity effects. Also, the effects of the different porosity models on the FG beams are investigated in post-buckling case.

Keywords: post-buckling; functionally graded material; porosity; total Lagragian; finite element method

1. Introduction

Functionally graded materials (FGMs) are a new generation of composites where the volume fraction of the FGM constituents vary gradually, giving a non-uniform microstructure with continuously graded macro properties such as elasticity modulus, density, heat conductivity, etc.. Typically, in an FGM, one face of a structural component is ceramic that can resist severe thermal loading and the other face is metal which has excellent structural strength. FGMs consisting of heat-resisting ceramic and fracture-resisting metal can improve the properties of thermal barrier systems because cracking and delamination, which are often observed in conventional layered composites, are reduced by proper smooth transition of material properties. FGMs have many practical applications, such as reactor vessels, biomedical sectors, aircrafts, space vehicles, defense industries and other engineering structures.

In the literature, much more attention has been given to the linear analysis of FG beam structures. However, post-buckling and nonlinear studies of FG beams are very limited. In the open literature, studies of the post-buckling and nonlinear behavior of beams are as follows; The thermal buckling load of a curved beam made of FGM with doubly symmetric cross section was investigated by Rastgo *et al*. (2005). Agarwl *et al*. (2006) analysed the large deformation behaviour of anisotropic and inhomogeneous beams using exact linear static solutions. Li *et al*. (2006) examined the thermal post-buckling of FGM clamped-clamped Timoshenko beams subjected to transversely non-uniform temperature. Based on Kirchhoff's assumption of straight normal line of beams and considering the effects of the axial elongation, the initial curvature and stretching-bending coupling on the arch deformation, geometrically nonlinear governing equations of FGM arches subjected to mechanical and thermal loads were derived by Song and Li (2008). Kang and Li (2009) studied the bending of FGM cantilever beams with power-law non-linearity subjected to an end force. Ke *et al*. (2009) investigated the post-buckling of FGM beams with an open edge crack based on the Timoshenko beam theory and von Kármán nonlinear kinematics by using the Ritz method. Kang and Li (2010) examined the large deflections of a non-linear cantilever FGM beam. Hosseini and Fazelzadeh (2010) and Marzocca *et al*. (2011) investigated nonlinear aerothermoelastic nonlinear behavior of FG panels. The thermal post-buckling behaviour of uniform slender FGM beams was investigated independently using the classical Rayleigh-Ritz formulation and versatile finite element analysis based on the von Karman strain-displacement relations by Anandrao *et al*. (2010). Kocatürk *et al*. (2011) investigated the full geometrically non-linear static analysis of a cantilever Timoshenko beam composed of FGM under a non-follower transversal uniformly distributed load. Fallah and Aghdam (2011) studied the nonlinear free vibration and post-buckling analysis of FGM beams on nonlinear elastic foundation. Akbaş and Kocatürk (2011, 2012) investigated post-buckling of the beams under thermal effects. Almeida *et al*. (2011) conducted the geometric nonlinear analyses of FGM beams by using a tailored Lagrangian formulation. The thermomechanical stability of FG thin-walled cantilever pipes conveying flow and loading by compressive axial force was investigated by Hosseini and Fazelzadeh (2011). Li and Li (2011) analyzed post-buckling behavior of FG columns under distributed loads. Yan *et al*. (2012) investigated the nonlinear flexural dynamic behavior of a clamped Timoshenko beam made of FGM with an open edge crack under an axial parametric excitation, composed of a static compressive force and a harmonic excitation force based on the Timoshenko beam theory and von

*Corresponding author, Associate Professor,
E-mail: serefda@yahoo.com

ISSN: 1229-9367 (Print), 1598-6233 (Online)

Kármán nonlinear kinematics.

Mohanty *et al.* (2012) studied static and dynamic stability of FG ordinary and sandwich beams by uisng finite element method based on the Timoshenko beam theory. Kocatürk and Akbaş (2011, 2012) presented the post-buckling analysis of homogeneous and FG Timoshenko beams under thermal loadings. Akbaş and Kocatürk (2013) presented post-buckling analysis of FGM three-dimensional beams under the influence of temperature. Kocatürk and Akbaş (2013) investigated the thermal post-buckling of FG beams considering the temperature-dependent physical properties. Akbaş (2013) presented the geometrically nonlinear static analysis of edge cracked FGM Timoshenko beams subjected to a non-follower transversal point load. Nonlinear bending and thermal post-buckling of FG beams resting on an elastic foundation investigated by (Hui-Shen and Wang 2014, Li and Shao 2014, Zhang and Zhou 2014, Sun *et al.* 2016, Trinh *et al.* 2016). Babilio (2014) investigated the nonlinear dynamics of FG beams resting on a linear viscoelastic foundation under the axial time-dependent excitation. Nguyen *et al.* (2014) analyzed geometrically nonlinear of FG planar beam and frame structures by using finite element method. Akbaş (2015a, b) analyzed post-buckling of cracked and axially graded FG beams. Elmaguiri *et al.* (2015) studied the large-amplitude free vibration of clamped immovable thin FG beams. Kolakowski and Teter (2015) studied static coupled buckling of thin-walled FG columns with trapezoidal and square cross-sections. Amara *et al.* (2016) investigated post-buckling of simply supported FG beams using various shear deformation theories. Akbarzadeh Khorshidi *et al.* (2016) analyzed post-buckling of shear deformable FG nanobeams based on modified couple stress theory with von-Karman geometric nonlinearity. Kar and Panda (2016) examined the nonlinear free vibration of FG panels under nonlinear temperature field.

During the processing in the fabrication of functionally graded materials, it can occur micro-voids and porosities in the material body due to technically problems, curing or poor quality productions. Especially, the part of ceramic in the functionally graded materials occurs voids more frequently. It is known that the porosity is defined a measure of voids which a fraction of the volume of voids on the total volume. The porosity varies between 0 and 1. The porosity is very important issue in the mechanical behavior of structures. Material or structural elements can lose their strength after a certain porosity ratio. It is known that porosity in structural elements, becomes more flexible and its buckling, dynamic and static behaviors will be changed. Porosity cause changes in structural stiffness. Therefore, understanding the mechanical behavior and the safe performance of porosity structures are importance in designs.

In the literature, studies of the porosity effect in the FG structures are as follows; Wattanasakulpong and Ungbhakorn (2014) studied linear and nonlinear vibration FG beams with porosity effects. Mechab *et al.* (2016a, b) examined free vibration analysis of a FG nano-plate resting on elastic foundations with the porosities effect. Chen *et al.* (2015) studied buckling and bending of FG beams. Şimşek and Aydın (2017) examined forced vibration of FG microplates with porosity effects based on the modified couple stress theory. Jahwari and Naguib (2016) investigated FG viscoelastic porous plates with a higher order plate theory and statistical based model of cellular distribution. Vibration characteristics of FG beams with porosity effect and various thermal loadings are investigated by (Ebrahimi and Jafari 2016, Ebrahimi *et al.* 2016).

As seen from literature, post-buckling behavior of FG beams with porosity effects has not been investigated so far. The primary purpose of this study is to fill this gap for FG beams.

In the present study, the post-buckling analysis of a FG beam studied with porosity effect. The considered problem is solved by using the total Lagrangian finite element model of two dimensional (2-D) continuum by taking into account full geometric nonlinearity.

The effects of material distribution, compression loads and porosity parameters on the post-buckling responses FG beams are investigated with different porosity models. Also, the difference between of the porosity models is investigated in detail.

2. Theory and formulation

A simply supported FG beam of length L, width b, and height h, subjected to a compressive point load (F) at the left end as shown in Fig. 1 with material or Lagrangian coordinate system (x, y, z) and with spatial or Euler coordinate system (X, Y, Z). The FG beam is made porous materials and vary though height direction. It is assumed that the bottom surface of the FG beam is metal rich, whereas the top surface of the FG beam is ceramic rich.

The effective material properties of the FG beam, P, i.e., Young's modulus E, Poisson's ratio v and shear modulus G vary continuously in the thickness direction (Y axis) according to a power-law function as follows

$$P(Y) = \left(P_c - P_m\right)\left(\frac{Y}{h} + \frac{1}{2}\right)^k + P_m \tag{1}$$

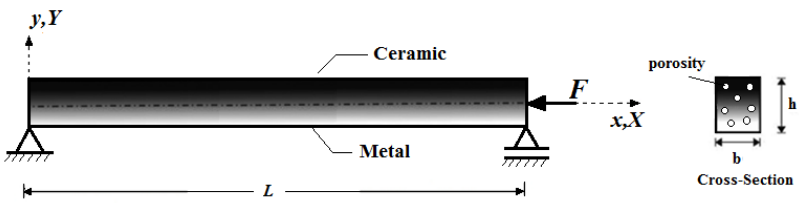

Fig. 1 A simply supported FG beam with porosity subjected to a compressive point load

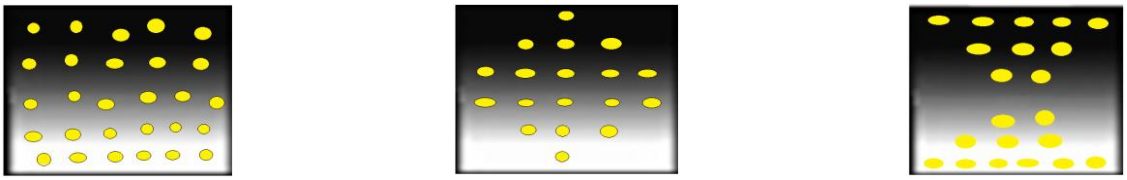

(a) Even porosity model (b) Uneven-1 porosity model (c) Uneven-2 porosity model

Fig. 2 Porosity models for FG material

where P_m and P_c are the material properties of the metal and the ceramic surfaces of the beam, k is the non-negative power-law exponent (material distribution parameter) which dictates the material variation profile through the thickness of the beam. It is clear from Eq. (1) that when $Y = -h/2$, $P = P_m$, and when $Y = h/2$, $P = P_c$. when $k = 0$ (full ceramic) or $k = \infty$ (full metal), the material of the beam is homogeneous according to Eq. (1).

In the porosity effect for imperfect FG beam, three porosities models (even, uneven-1 and uneven-2) are used which of some was given by Wattanasakulpong and Ungbhakorn (2014) for the power law distribution. In the even porosity model, the porosity spread uniformly though height direction. In the uneven-1 and uneven-2 porosity models, the porosity spread functionally though height direction. The distributions of the even, uneven-1 and uneven-2 porosity distributions are shown in Fig. 2.

According to the power law distribution, the effective material property for the even porosity can be expressed as follows

$$P(Y) = (P_c - P_m)\left(\frac{Y}{h} + \frac{1}{2}\right)^k + P_m - (P_m + P_c)\frac{a}{2} \tag{2}$$

where a ($a << 1$) is the volume fraction of porosities. When $a = 0$, the beam becomes perfect FGM.

The effective material property of uneven-1 and uneven-2 porosity distributions can be expressed in the Eqs. (3a) and (3b) respectively, according to the power law distribution

$$P(Y) = (P_c - P_m)\left(\frac{Y}{h} + \frac{1}{2}\right)^k + P_m - (P_m + P_c)\frac{a}{2}\left(1 - \frac{2\,|\,Y|}{h}\right) \tag{3a}$$

$$P(Y) = (P_c - P_m)\left(\frac{Y}{h} + \frac{1}{2}\right)^k + P_m - (P_m + P_c)\frac{a}{2}\left(\frac{2\,|\,Y|}{h}\right) \tag{3b}$$

In the comparison of the three porosity models: In uneven-1 porosity model, the voids stack in the middle of the beam or the neutral of the beam. So, the stiffness of the cross-section is less effected from negative influences of the porosity because the neutral axis and its adjacent areas have low stress. However, the voids stack in the upper and lower surfaces of the beam in the uneven-2 porosity model and consequently, the stiffness of the cross-section seriously decreases because the upper and lower surfaces of the beam have high stresses and strains. Therefore, the rigidity of the beam in uneven-2 porosity model is lower than the rigidity of the beam in uneven-1 porosity model.

In even porosity model, the voids stack uniformly in the whole area of the beam. So, pore space in the even porosity model is more than uneven models'. As result, the rigidity of the beam in even porosity model is lower than the rigidity of the beam in uneven porosity models.

It is known that the post-buckling case is a geometrically nonlinear problem. In the nonlinear kinematic model of the beam for the post-buckling problem, total Lagrangian approximation is used within the 2-D solid continuum model. In the solution of the nonlinear problem, finite element method is used for total Lagrangian kinematic model for an eight-node quadratic element.

The total Lagrangian finite element formulations of the problem are developed for porosity FGM beam by using the formulations given by Reddy (2004) and for isotropic and homogeneous beam material.

The constitutive relation between the second Piola-Kirchhoff stress tensor and the Green-Lagrange strain tensor can be expressed as follows

$$ {}^1_0S = \begin{Bmatrix} {}^1_0S_{11} \\ {}^1_0S_{22} \\ {}^1_0S_{12} \end{Bmatrix} = \begin{bmatrix} {}_0C_{11} & {}_0C_{12} & 0 \\ {}_0C_{12} & {}_0C_{22} & 0 \\ 0 & 0 & {}_0C_{66} \end{bmatrix} \begin{Bmatrix} {}^1_0E_{11} \\ {}^1_0E_{22} \\ 2\,{}^1_0E_{12} \end{Bmatrix} \tag{4}$$

where ${}^1_0S_{11}$, ${}^1_0S_{22}$, ${}^1_0S_{12}$ are the components of the second Piola-Kirchhoff stress tensor components in the initial configuration of the body, ${}^1_0E_{ij}$ are the components of the Green-Lagrange strain tensor, ${}_0C_{ij}$ are the components of the reduced constitutive tensor in the initial configuration of the body. The components of the reduced constitutive tensor can be written in terms of Young modulus E and Poisson's ratio v and their dependence on Y coordinate are given by Eqs. (2) and (3) for porosity effect as follows

$$ {}_0C_{11} = \frac{E(Y)}{1 - v^2(Y)}\ ,\ {}_0C_{12} = {}_0C_{21} = \frac{v(Y)E(Y)}{1 - v^2(Y)}\ , \quad {}_0C_{22} = \frac{E(Y)}{1 - v^2(Y)}\ ,\ {}_0C_{66} = \frac{E(Y)}{2(1 + v(Y))} \tag{5}$$

The Green-Lagrange strain tensor is expressed in terms of displacements in the case of two-dimensional solid continuum as follows

$$ {}^1_0E = \begin{Bmatrix} {}^1_0E_{11} \\ {}^1_0E_{22} \\ 2\,{}^1_0E_{12} \end{Bmatrix} = \begin{Bmatrix} \dfrac{\partial u}{\partial X} + \dfrac{1}{2}\left[\left(\dfrac{\partial u}{\partial X}\right)^2 + \left(\dfrac{\partial v}{\partial X}\right)^2\right] \\ \dfrac{\partial v}{\partial Y} + \dfrac{1}{2}\left[\left(\dfrac{\partial u}{\partial Y}\right)^2 + \left(\dfrac{\partial v}{\partial Y}\right)^2\right] \\ \dfrac{\partial u}{\partial Y} + \dfrac{\partial v}{\partial X} + \dfrac{1}{2}\left[\dfrac{\partial u}{\partial X}\dfrac{\partial u}{\partial Y} + \dfrac{\partial v}{\partial X}\dfrac{\partial v}{\partial Y}\right] \end{Bmatrix} \tag{6}$$

In the finite element model, eight-node plane element is

used as shown in Fig. 3.

These total displacement fields and incremental displacement fields are interpolated as follows

$$\{u\} = \begin{Bmatrix} u \\ v \end{Bmatrix} = \begin{Bmatrix} \sum_{j=1}^{8} u_j \psi_j(x) \\ \sum_{j=1}^{8} v_j \psi_j(x) \end{Bmatrix} = [\Psi][\Delta] \tag{7}$$

$$\{\bar{u}\} = \begin{Bmatrix} \bar{u} \\ \bar{v} \end{Bmatrix} = \begin{Bmatrix} \sum_{j=1}^{8} \bar{u}_j \psi_j(x) \\ \sum_{j=1}^{8} \bar{v}_j \psi_j(x) \end{Bmatrix} = [\bar{\Psi}][du] \tag{8}$$

where

$$[\Psi] = \begin{bmatrix} \psi_1\ 0\ \psi_2\ 0\ \psi_3\ 0\ \psi_4\ 0\ \psi_5\ 0\ \psi_6\ 0\ \psi_7\ 0\ \psi_8\ 0 \\ 0\ \psi_1\ 0\ \psi_2\ 0\ 0\ \psi_4\ 0\ \psi_5\ 0\ \psi_6\ 0\ \psi_7\ 0\ \psi_8\ 0 \end{bmatrix} \tag{9}$$

$$\{\mathrm{D}\}^T = \{u_1\ v_1\ u_2\ v_2\ u_3\ v_3\ u_4\ v_4\ u_5\ v_5\ u_6\ v_6\ u_7\ v_7\ u_8\ v_8\} \tag{10}$$

$$\{\mathrm{du}\}^T = \{\bar{u}_1\ \bar{v}_1\ \bar{u}_2\ \bar{v}_2\ \bar{u}_3\ \bar{v}_3\ \bar{u}_4\ \bar{v}_4\ \bar{u}_5\ \bar{v}_5\ \bar{u}_6\ \bar{v}_6\ \bar{u}_7\ \bar{v}_7\ \bar{u}_8\ \bar{v}_8\} \tag{11}$$

The tangent stiffness matrix K_T^i and the residual vector R_{n+1}^i which are to be used in Eq. (15) at the ith iteration for the total Lagrangian finite element model of two dimensional continua for an eight-node quadratic element are given below

$$\begin{bmatrix} K^{11L} + K^{11NL} & K^{12L} \\ K^{21L} & K^{22L} + K^{22NL} \end{bmatrix}^i \begin{Bmatrix} \bar{u} \\ \bar{v} \end{Bmatrix}^i = \begin{Bmatrix} {}_0^2F^1 - {}_0^1F^1 \\ {}_0^2F^2 - {}_0^1F^2 \end{Bmatrix}^i \tag{12}$$

where

$$K_{ij}^{11L} = b\int_A \left\{ {}_0C_{11}\left(1+\frac{\partial u}{\partial X}\right)^2 \frac{\partial \psi_i}{\partial X}\frac{\partial \psi_j}{\partial X} + {}_0C_{22}\left(\frac{\partial u}{\partial Y}\right)^2 \frac{\partial \psi_i}{\partial Y}\frac{\partial \psi_j}{\partial Y} + {}_0C_{12}\left(1+\frac{\partial u}{\partial X}\right)\left(\frac{\partial \psi_i}{\partial X}\frac{\partial \psi_j}{\partial X} + \frac{\partial \psi_i}{\partial Y}\frac{\partial \psi_j}{\partial X}\right) + {}_0C_{66}\left[\left(1+\frac{\partial u}{\partial X}\right)\frac{\partial \psi_i}{\partial Y} + \frac{\partial u}{\partial Y}\frac{\partial \psi_j}{\partial X}\right] \times \left[\left(1+\frac{\partial u}{\partial X}\right)\frac{\partial \psi_j}{\partial Y} + \frac{\partial u}{\partial Y}\frac{\partial \psi_j}{\partial X}\right]\right\} dXdY \tag{13a}$$

$$K_{ij}^{12L} = b\int_A \left\{ {}_0C_{11}\left(1+\frac{\partial u}{\partial X}\right)\frac{\partial v}{\partial X}\frac{\partial \psi_i}{\partial X}\frac{\partial \psi_j}{\partial X} + {}_0C_{22}\left(1+\frac{\partial v}{\partial Y}\right)\frac{\partial u}{\partial Y}\frac{\partial \psi_i}{\partial Y}\frac{\partial \psi_j}{\partial Y} + {}_0C_{12}\left[\left(1+\frac{\partial u}{\partial X}\right)\left(1+\frac{\partial v}{\partial Y}\right)\frac{\partial \psi_i}{\partial X}\frac{\partial \psi_j}{\partial Y} + \frac{\partial u}{\partial Y}\frac{\partial v}{\partial X}\frac{\partial \psi_i}{\partial Y}\frac{\partial \psi_j}{\partial X}\right] + {}_0C_{66}\left[\left(1+\frac{\partial u}{\partial X}\right)\frac{\partial \psi_i}{\partial Y} + \frac{\partial u}{\partial Y}\frac{\partial \psi_i}{\partial X}\right] \times \left[\left(1+\frac{\partial v}{\partial Y}\right)\frac{\partial \psi_j}{\partial X} + \frac{\partial v}{\partial X}\frac{\partial \psi_j}{\partial Y}\right]\right\} dXdY \tag{13b}$$

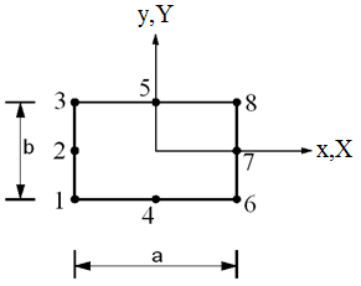

Fig. 3 Eight-node plane element

$$= K_{ij}^{21L}$$

$$K_{ij}^{22L} = b\int_A \left\{ {}_0C_{11}\left(\frac{\partial v}{\partial X}\right)^2 \frac{\partial \psi_i}{\partial X}\frac{\partial \psi_j}{\partial X} + {}_0C_{22}\left(1+\frac{\partial v}{\partial Y}\right)^2 \frac{\partial \psi_i}{\partial Y}\frac{\partial \psi_j}{\partial Y} + {}_0C_{12}\left(1+\frac{\partial v}{\partial Y}\right)\frac{\partial v}{\partial X}\left(\frac{\partial \psi_i}{\partial X}\frac{\partial \psi_j}{\partial X} + \frac{\partial \psi_i}{\partial Y}\frac{\partial \psi_j}{\partial X}\right) + {}_0C_{66}\left[\left(1+\frac{\partial v}{\partial Y}\right)\frac{\partial \psi_i}{\partial X} + \frac{\partial v}{\partial X}\frac{\partial \psi_j}{\partial Y}\right] \times \left[\left(1+\frac{\partial v}{\partial Y}\right)\frac{\partial \psi_j}{\partial X} + \frac{\partial v}{\partial X}\frac{\partial \psi_j}{\partial Y}\right]\right\} dXdY \tag{13c}$$

$$K_{ij}^{11NL} = K_{ij}^{22NL} = b\int_A \left\{ {}_0^1S_{11}\frac{\partial \psi_i}{\partial X}\frac{\partial \psi_j}{\partial X} + {}_0^1S_{12}\left(\frac{\partial \psi_i}{\partial Y}\frac{\partial \psi_j}{\partial X} + \frac{\partial \psi_i}{\partial X}\frac{\partial \psi_j}{\partial Y}\right) + {}_0^1S_{22}\frac{\partial \psi_i}{\partial Y}\frac{\partial \psi_j}{\partial Y}\right\} dXdY \tag{13d}$$

$${}_0^2F_i^1 = b\int_A {}_0^2f_x\,\psi_i dXdY + \int_\Gamma {}_0^2t_x\,\psi_i ds \tag{13e}$$

$${}_0^2F_i^2 = b\int_A {}_0^2f_y\,\psi_i dXdY \int_\Gamma {}_0^2t_y\,\psi_i ds \tag{13f}$$

where ${}_0^2f_x$, ${}_0^2f_y$ are the body forces, ${}_0^2t_x$, ${}_0^2t_y$ are the surface forces in the x and y directions. u and v are displacements in the x and y directions, ψ indicates the shape functions.

$${}_0^1F_i^1 = b\int_A \left\{ {}_0^1S_{11}\left(1+\frac{\partial u}{\partial X}\right)\frac{\partial \psi_i}{\partial X} + {}_0^1S_{22}\frac{\partial u}{\partial Y}\frac{\partial \psi_i}{\partial Y} + {}_0^1S_{12}\left[\left(1+\frac{\partial u}{\partial X}\right)\frac{\partial \psi_i}{\partial Y} + \frac{\partial u}{\partial Y}\frac{\partial \psi_i}{\partial Y}\right]\right\} dXdY \tag{14a}$$

$${}_0^1F_i^2 \tag{14b}$$

$$= b \int_A \left\{ {}_0^1S_{11} \frac{\partial v}{\partial X}\frac{\partial \psi_i}{\partial X} + {}_0^1S_{22}\left(1+\frac{\partial v}{\partial Y}\right)\frac{\partial \psi_i}{\partial Y} + {}_0^1S_{12}\left[\left(1+\frac{\partial v}{\partial Y}\right)\frac{\partial \psi_i}{\partial X} + \frac{\partial v}{\partial X}\frac{\partial \psi_i}{\partial Y}\right]\right\} dXdY \tag{14b}$$

For the solution of the nonlinear finite element of total Lagrangian formulations, small-step incremental approaches from known solutions are used. In the iterations, the load is divided by a suitable number according to the value of load. The loading is divided by large numbers. After completing an iteration process, the load is increased by adding load increment to the accumulated load.

In the solution of the nonlinear problem, Newton-Raphson iteration method is used in which the solution for n+1th load increment and ith iteration is obtained in the following form

$$\mathrm{d}\mathbf{u}_n^i = (\mathbf{K}_T^i)^{-1}\mathbf{R}_{n+1}^i \tag{15}$$

Where K_T^i is the tangent stiffness matrix corresponding to a tangent direction at the ith iteration, du_n^i is the solution increment vector at the ith iteration and n+1th load increment, R_{n+1}^i is the residual vector at the ith iteration and n+1th load increment. This iteration procedure is continued until the difference between two successive solution vectors is less than a selected tolerance criterion in Euclidean norm given by

$$\sqrt{\frac{[(du_n^{i+1}-du_n^i)^T(du_n^{i+1}-du_n^i)]^2}{[(du_n^{i+1})^T(du_n^{i+1})]^2}} \le \zeta_{tol} \tag{16}$$

A series of successive approximations gives

$$\mathbf{u}_{n+1}^{i+1} = \mathbf{u}_{n+1}^i + \mathrm{d}\mathbf{u}_{n+1}^i = \mathbf{u}_n + \mathrm{D}\mathbf{u}_n^i \tag{17}$$

where

$$\Delta u_n^i = \sum_{k=1}^{i} du_n^k \tag{18}$$

Shape functions for an eight-node element are as follows

$$[\psi_1] = \left(X-\frac{a}{2}\right)\left(Y-\frac{b}{2}\right)\left(-\frac{1}{ab}-\frac{2X}{a^2b}-\frac{2Y}{ab^2}\right)$$
$$[\psi_2] = \left(\frac{4}{ab^2}\right)\left(X-\frac{a}{2}\right)\left(Y+\frac{b}{2}\right)\left(Y-\frac{b}{2}\right)$$
$$[\psi_3] = \left(X-\frac{a}{2}\right)\left(Y+\frac{b}{2}\right)\left(\frac{1}{ab}+\frac{2X}{a^2b}-\frac{2Y}{ab^2}\right)$$
$$[\psi_4] = \left(\frac{4}{ba^2}\right)\left(X-\frac{a}{2}\right)\left(X+\frac{a}{2}\right)\left(Y-\frac{b}{2}\right)$$
$$[\psi_5] = \left(\frac{4}{ba^2}\right)\left(X-\frac{a}{2}\right)\left(X+\frac{a}{2}\right)\left(Y+\frac{b}{2}\right)$$
$$[\psi_6] = \left(X+\frac{a}{2}\right)\left(Y-\frac{b}{2}\right)\left(\frac{1}{ab}-\frac{2X}{a^2b}+\frac{2Y}{ab^2}\right)$$
$$[\psi_7] = \left(-\frac{4}{ab^2}\right)\left(X+\frac{a}{2}\right)\left(Y+\frac{b}{2}\right)\left(Y-\frac{b}{2}\right)$$
$$[\psi_8] = \left(X+\frac{a}{2}\right)\left(Y+\frac{b}{2}\right)\left(-\frac{1}{ab}+\frac{2X}{a^2b}+\frac{2Y}{ab^2}\right) \tag{19}$$

3. Numerical results

In the numerical examples, post-buckling deflections of the simply supported FG beam are calculated and presented for different power-law exponents and porosity coefficients under compressive point load (F) at the right end of the beam (Fig. 1). The difference between of the porosity models is investigated in post-buckling case. Using the conventional assembly procedure for the finite elements, the tangent stiffness matrix and the residual vector are obtained from the element stiffness matrices and residual vectors in the total Lagrangian sense for finite element model of 2-D solid continuum. After that, the solution process outlined in the preceding section is used to obtain the solution for the problem of concern. In obtaining the numerical results, graphs and solution of the nonlinear finite element model, MATLAB program is used. Numerical calculations of the integrals seen in the rigidity matrices will be performed by using five-point Gauss rule.

The FG porous beam considered in numerical examples is made of metal material; Aluminum (Al; E = 70 GPa, ν = 0.3) and ceramic material: Alumina (Al_2O_3 ; E = 380 GPa, ν = 0.3). The bottom surface of the FG beam is metal rich (Aluminum), whereas the top surface of the FG beam is ceramic rich (Alumina). When k = 0 and k = ∞, the material of the beam gets homogeneous Alumina and homogeneous Aluminum, respectively, according to Eq. (2) and Eq. (3). The dimensions of the beam are considered as follows:

b = 0.2 m, h = 0.2 m, L = 5 m in the numerical examples.

In order to obtain the optimum number of the finite element for the numerical calculations, the convergence study is performed in Fig. 4. In Fig. 4, post-buckling maximum vertical displacements (at the midpoint of the beam) of the FG porous beam (v_{max}) are calculated for different numbers of finite elements for the compressive point load F = 10000 kN, the power-law exponent k = 0.5, the porosity parameter a = 0.2 for even porosity model. It is

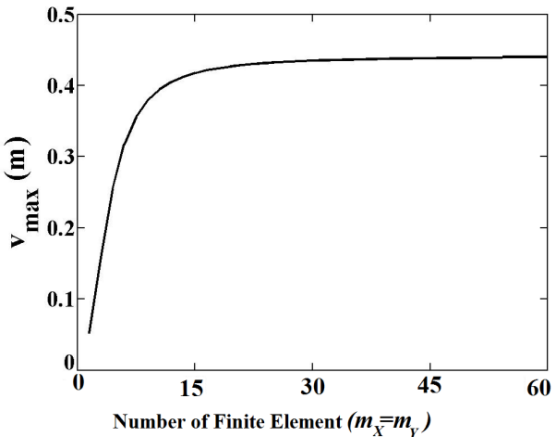

Fig. 4 Convergence study for post-buckling vertical displacements at the midpoint of the FG porous beam

Table 1 Dimensionless critical buckling load of non-porous simple supported FG beam for different material distribution and L/h ratios

Porosity model	L/h	k	Present	Amara *et al*. (2016)
Porosity distribution 1	L/h = 20	k = 0.3	3.801	3.791
		k = 1	2.894	2.888
		k = 3	2.296	2.288
		k = 5	2.041	2.032
		k = 10	1.685	1.674
Porosity distribution 2	L/h = 50	k = 0.3	3.811	3.809
		k = 1	2.903	2.902
		k = 3	2.302	2.302
		k = 5	2.046	2.045
		k = 10	1.686	1.685

Table 2 Dimensionless critical buckling load of porous simple supported beam for L/h = 20 and e_0 = 0.5

Porosity nodel	Present	Chen *et al*. (2015)
Porosity distribution 1	0.0033389	0.0033387
Porosity distribution 2	0.0028692	0.0028688

noted that the finite element of the FG beam is chosen to be equal in X and Y directions in order to obtain sensitive results. In Fig. 4, m_X and m_Y indicate the number of finite element in X and Y directions, respectively.

Fig. 4 shows that the post-buckling maximum displacements converge perfectly after the finite element $m_X = m_Y$ = 30. So, the number of finite elements is taken as 30 in both X and Y directions in the numerical calculations.

In order to establish the accuracy of the present formulation and the computer program developed by the author, the results obtained from the present study are compared with the available results in the literature. For this purpose, the dimensionless critical buckling loads of a FG simply supported beam without porosity are calculated for various material distribution parameters k and L/h ratios compared with those of Amara *et al*. (2016) in the Timoshenko beam theory in Table 1. As seen from Table 1, the present results are in good agreement with that the results of Amara *et al* (2016).

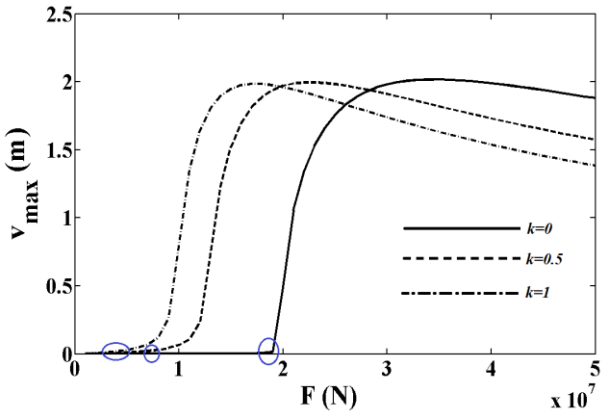

Fig. 5 Compressive load-the maximum vertical displacements (v_{max}) curves for different the material distribution parameter k

To further verify the present results, the dimensionless critical buckling loads with porosity coefficient are calculated and compared with those of Chen *et al*. (2015) for different trigonometric porosity distributions according to Timoshenko beam theory in Table 2. The material and geometry parameter used in Chen *et al*. (2015) are; E = 200 GPa, v_u = 0.33, b = 0.1 m, h = 0.1 m, the material properties of the beam change according to a trigonometric function. In Table 2, e_0 indicates the porosity parameter according to the study of Chen *et al*. (2015). It is seen from Table 2, the present results are close to the results of Chen *et al*. (2015).

It is noted that, the results in the Tables 1 and 2 are obtained according to the porosity models of Chen *et al*. (2015) and Amara *et al*. (2016).

In Fig. 5, the effect of the material distribution parameter k on the post-buckling deflections of the FG beam is presented for a = 0.

In Fig. 5, furcation points can be seen (see circle). It is known that buckling case occurs at the furcation points: Actually these points are bifurcation points. As it is known, according to the initial arbitrary deviation from the straight position of the beam, buckling can occur in either positive or negative directions. In this study, deviation from the straight position is always taken as positive for buckling analysis. The symmetrical branches according to load axis would be obtained if the deviations from the straight positions were taken as negative values. It is seen Fig. 5 that with increase in load, the responses of the beams converge. This situation may be explained as follows: the arm of the external forces change with the magnitude of the external force and, as the magnitude of the force increases the arm of these external forces decrease. However, as the forces increase the configuration of the beam become close to vertical direction and therefore increase in the load does not cause a significant increase in displacements after certain load level in which the configuration of the beam is close to the vertical direction. This situation is seen in Figs. 9 and 10 which show the displaced configuration of the beam. After this load, it is expected that axial rigidity of the beam gains more importance than its flexural rigidity.

Also, it is seen from Fig. 5 that increase in the k causes a decrease in the critical buckling loading (see furcation points). With increase in the k, the beam gets to full Aluminum. The Young modulus of the Aluminum is smaller than Alumina's. This is as expected, due to the fact that an increase in the k can increase the elasticity modulus and bending rigidity of the beam decrease according to Eqs. (2) and (3). As a result, the strength of the material decreases and the critical buckling load decreases naturally.

In order to investigate the effect of porosity parameter (a) and porosity models on the post-buckling responses of the FG porous beam, the maximum transverse displacements (v_{max}) obtained and illustrated versus compressive load rising (F) in Fig. 6 for the power-law exponent k = 10.

It is seen from Fig. 6 that the results of the even porosity model are bigger than uneven models'. It is mentioned

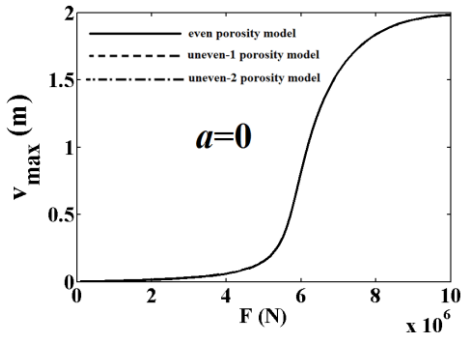

(a) For a = 0 (Perfect FG beam)

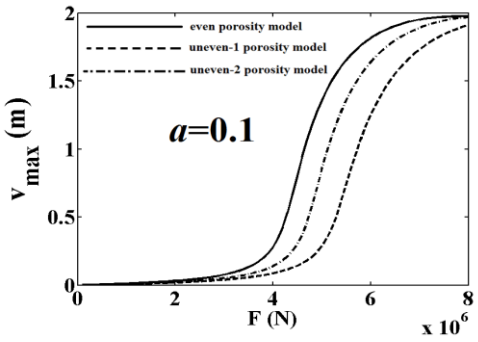

(b) For a = 0.1

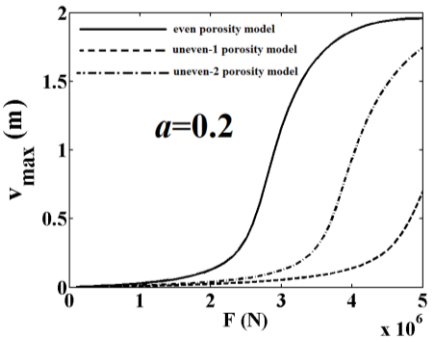

(c) For a = 0.2

Fig. 6 Load-the maximum vertical displacements (v_{max}) curves rising compressive loads for different the porosity parameters

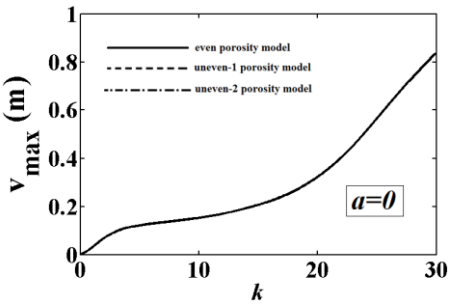

(a) For a = 0 (Perfect FG beam)

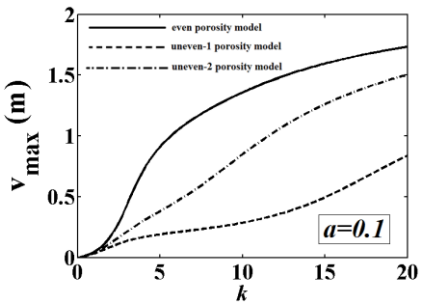

(b) For a = 0.1

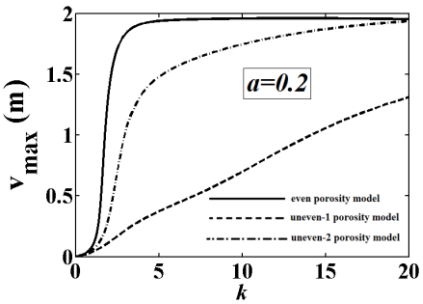

(c) For a = 0.2

Fig. 7 The relationship between of the maximum vertical displacements and the material distribution parameter k in the post-buckling case of the FG porous beam

before that, the rigidity of the beam in even porosity model is lower than the rigidity of the beam in uneven porosity models. So, the post-buckling deflections in even porosity model are bigger than uneven models'. In addition, the post-buckling deflections of uneven-2 porosity model are bigger than uneven-1 model. This is because: the rigidity of the beam in uneven-2 porosity model is lower than the rigidity of the beam in uneven-1 porosity model. In Fig.

6(a), the results of the three models coincide with each other in case of a = 0 (perfect FG beam) because the porosity effect is not considered. Also, it is seen from figure 6 that the increase in compressive load causes increase in difference of the porosity models.

Another result of Fig. 6 that the increase in porosity parameter a causes decrease in critical buckling load (see furcation points). This is because, with increase in the porosity parameter, the intermolecular distances of the material increase and intermolecular forces decrease. As a result, the strength of the material decreases and the critical buckling load decreases naturally. In addition, the critical buckling load for the even porosity model are smaller than uneven model's as seen from Fig. 6.

Fig. 7 shows the relationship between of porosity parameter a and the material distribution parameter k in the post-buckling deflections in three porosity models for the value of the compressive load F = 5000 kN.

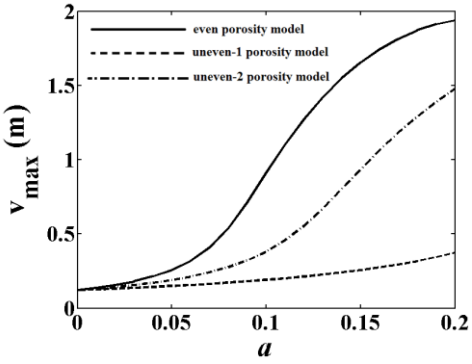

Fig. 8 The effect of porosity parameter (a) and porosity models on the maximum vertical displacements of the FG porous beam

As seen from Fig. 7, increase in the k causes increase in the displacements. It is mentioned before that, with increase in the k, rigidity of the beam decrease according to Eqs. (2) and (3). The difference between the even and uneven porosity models increases with increase in k parameter. Especially, the difference of three models is quite large in the medium values of k. In the medium values of k, the inhomogeneous level is quite large according to Eqs. (2) and (3). It can be concluded from Fig. 7 that the porosity is very effective in the mechanical behavior of beams in the medium values of k. However, the difference of the three models can be neglect in full k = 0 (homogeneous Alumina) or $k = \infty$ (homogeneous Aluminum). It can be concluded from here: with the suitable choice of material distribution parameter, the negative effects of the porosity can be reduced. It shows that the material distribution plays an important role on the mechanical behavior of the porous FGM beam.

Fig. 8 displays the relationship between of porosity parameter a and the maximum displacements of the FG porous beam for k = 5 and F = 5000 kN.

As seen from Fig. 8 that increase in the porosity parameter a, the difference between of porosity models increases considerably. In higher values of porosity parameter a, the difference of porosity models is quite large. It shows that the porosity parameters have a very important role on the mechanical behavior of the FG porous beam.

Fig. 9 shows that effect of material distribution parameter k on the post-buckling deflected shape of the FG

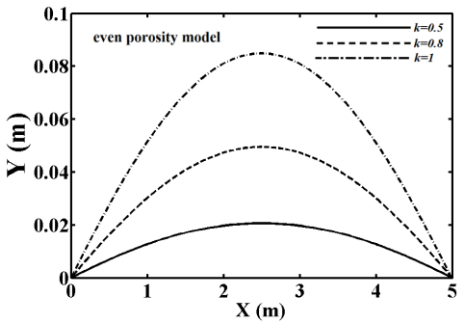

(a) For even porosity model

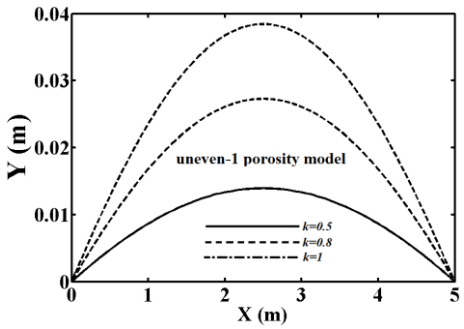

(b) For uneven-1 porosity model

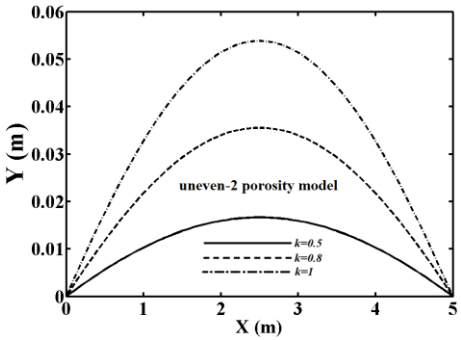

(c) For uneven-2 porosity model

Fig. 9 The effect of material distribution parameter k on the deflected shape of the FG porous beam for different porosity models

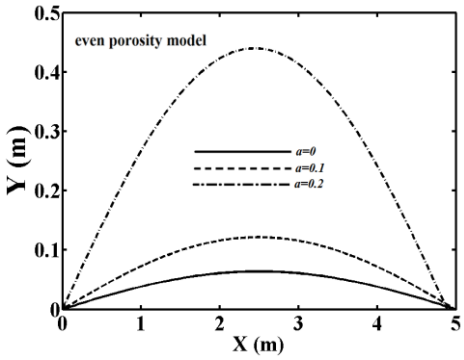

(a) For even porosity model

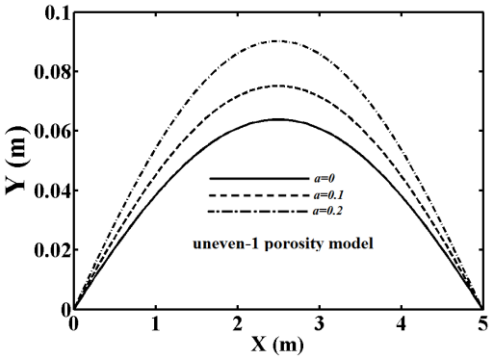

(b) For uneven-1 porosity model

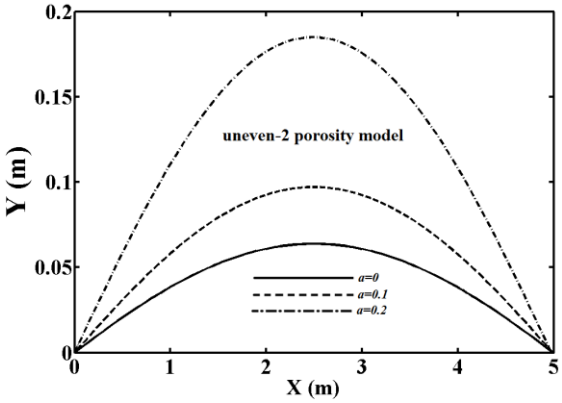

(c) For uneven-2 porosity model

Fig. 10 The effect of porosity parameter *a* on the deflected shape of the FG porous beam for different porosity models

porous beam for three porosity models, respectively for a = 0.2 and F = 5000 *kN*.

It is seen from Fig. 9 that different material distributions are very effective of the deflection of the beam. Increase in the *k*, the post-buckling deflections of the FG beam increase considerably. In the even porosity model, the beam more deflects in comparison with the uneven-1 and uneven-2 porosity models.

Fig. 10 displays that effect of porosity parameter a on the post-buckling deflected shape of the FG porous beam for three porosity models for k = 0.5 and F = 10000 kN.

It is seen from Fig. 10, the differences of porosity parameters in the even porosity model are bigger than the uneven models'. With increase in the *a*, the displacements of the FG beam increase significantly.

4. Conclusions

Post-buckling responses of a FG beam are investigated with porosity effect by using total Lagrangian finite element model of 2-D continuum. The effects of material distribution and porosity parameters on the post-buckling deflections of the FG porous beam are studied and discussed for different porosity models. The considered non-linear problem is solved by using incremental displacement-based finite element method in conjunction with Newton-Raphson iteration method. Convergence study was performed.

It is observed from the investigations, the main conclusions are as follows:

- The porosity has a very important role on the post-buckling behavior of the FG beam.
- Increase in the porosity parameter a and compressive load, the difference between the porosity models increases considerably.
- It is found that the critical buckling load in the even porosity model are smaller than uneven models'.
- The material distribution plays an important role on the post-buckling behavior of the porous FGM beam.
- With the suitable choice of material distribution parameter, the negative effects of the porosity can be reduced.

References

Agarwal, S., Chakraborty, A. and Gopalakrishnan, S. (2006), "Large deformation analysis for anisotropic and inhomogeneous beams using exact linear static solutions", *Compos. Struct.*, **72**(1), 91-104.

Akbarzadeh Khorshidi, M., Shariati, M. and Emam, S.A. (2016), "Postbuckling of functionally graded nanobeams based on modified couple stress theory under general beam theory", *Int. J. Mech. Sci.*, **110**(1), 160-169.

Akbaş, Ş.D. (2013), "Geometrically nonlinear static analysis of edge cracked Timoshenko Beams composed of functionally

graded material", *Math. Problems Eng*., 14 p. DOI: 10.1155/2013/871815

Akbaş, Ş.D. (2015a), "On post-buckling behavior of edge cracked functionally graded beams under axial loads", *Int. J. Struct. Stabil. Dyn*., **15**(4), 1450065. DOI: 10.1142/S0219455414500655

Akbaş, Ş.D. (2015b), "Post-buckling analysis of axially functionally graded three dimensional beams", *Int. J. Appl. Mech*., **7**(3), 1550047. DOI: 10.1142/S1758825115500477

Akbaş, Ş.D. and Kocatürk, T. (2011), "Post-buckling analysis of a simply supported beam under uniform thermal loading", *Sci. Res. Essays*, **6**(5), 1135-1142.

Akbaş, Ş.D. and Kocatürk, T. (2012), "Post-buckling analysis of Timoshenko beams with temperature-dependent physical properties under uniform thermal loading", *Struct. Eng. Mech, Int. J*., **44**(1), 109-125.

Akbaş, Ş.D. and Kocatürk, T. (2013), "Post-buckling analysis of functionally graded three- dimensional beams under the influence of temperature", *J. Thermal Stresses*, **36**(12), 1235-1254.

Al Jahwari, F. and Naguib, H.E. (2016), "Analysis and homogenization of functionally graded viscoelastic porous structures with a higher order plate theory and statistical based model of cellular distribution", *Appl. Math. Model*., **40**(3), 2190-2205.

Almeida, C.A., Albino, J.C.R., Menezes, I.F.M. and Paulino, G.H. (2011), "Geometric nonlinear analyses of functionally graded beams using a tailored Lagrangian formulation", *Mech. Res. Commun*., **38**(8), 553-559.

Amara, K., Bouazza, M. and Fouad, B. (2016), "Postbuckling analysis of functionally graded beams using nonlinear model", *Periodica Polytechnica. Eng. Mech. Eng*., **60**(2), 121-128.

Anandrao, K.S., Gupta, R.K., Ramchandran, P. and Rao, V. (2010), "Thermal post-buckling analysis of uniform slender functionally graded material beams", *Struct. Eng. Mech., Int. J*., **36**(5), 545-560.

Babilio, E. (2014), "Dynamics of functionally graded beams on viscoelastic foundation", *Int. J. Struct. Stabil. Dyn*., **14**(8), 1440014. DOI: 10.1142/S0219455414400148

Chen, D., Yang, J. and Kitipornchai, S. (2015), "Elastic buckling and static bending of shear deformable functionally graded porous beam", *Compos. Struct*., **133**(1), 54-61.

Ebrahimi, F. and Jafari, A. (2016), "A higher-order thermo-mechanical vibration analysis of temperature-dependent FGM beams with porosities", *J. Eng*., 20 p. DOI: 10.1155/2016/9561504

Ebrahimi, F. Ghasemi, F. and Salari, E. (2016), "Investigating thermal effects on vibration behavior of temperature-dependent compositionally graded Euler beams with porosities", *Meccanica*, **51**(1), 223-249.

Elmaguiri, M., Haterbouch, M., Bouayad, A. and Oussouaddi, O. (2015), "Geometrically nonlinear free vibration of functionally graded beams", *J. Mater. Environ. Sci*., **6**(12), 3620-3633.

Fallah, A. and Aghdam, M.M. (2011), "Nonlinear free vibration and post-buckling analysis of functionally graded beams on nonlinear elastic foundation", *Eur. J. Mech. - A/Solids*, **30**(4), 571-583.

Hosseini, M. and Fazelzadeh, S.A. (2010), "Aerothermoelastic post-critical and vibration analysis of temperature-dependent functionally graded panels", *J. Thermal Stresses*, **33**(12), 1188-1212.

Hosseini, M. and Fazelzadeh, S.A. (2011), "Thermomechanical stability analysis of functionally graded thin-walled cantilever pipe with flowing fluid subjected to axial load", *Int. J. Struct. Stabil. Dyn*., **11**(3), 513-534.

Hui-Shen, S. and Wang, Z.-X. (2014), "Nonlinear analysis of shear deformable FGM beams resting on elastic foundations in thermal environments", *Int. J. Mech. Sci*., **81**, 195-206.

Jahwari, F. and Naguib, H.E. (2016), "Analysis and homogenization of functionally graded viscoelastic porous structures with a higher order plate theory and statistical based model of cellular distribution", *Appl. Math. Model*., **40**(3), 2190-2205.

Kang, Y.A. and Li, X.F. (2009), "Bending of functionally graded cantilever beam with power-law non-linearity subjected to an end force", *Int. J. Non-Linear Mech*., **44**(6), 696-703.

Kang, Y.A. and Li, X.F. (2010), "Large deflections of a non-linear cantilever functionally graded beam", *J. Reinf. Plast. Compos*., **29**(12), 1761-1774.

Kar, V.R. and Panda, S.K. (2016), "Geometrical nonlinear free vibration analysis of FGM spherical panel under nonlinear thermal loading with TD and TID properties", *J. Thermal Stresses*, **39**(8), 942-959.

Ke, L.-L., Yang, J. and Kitipornchai, S. (2009), "Postbuckling analysis of edge cracked functionally graded Timoshenko beams under end shortening", *Compos. Struct*., **90**(2), 152-160.

Kocatürk, T. and Akbaş, Ş.D. (2011), "Post-buckling analysis of Timoshenko beams with various boundary conditions under non-uniform thermal loading", *Struct. Eng. Mech., Int. M*., **40**(3), 347-371.

Kocatürk, T. and Akbaş, Ş.D. (2012), "Post-buckling analysis of Timoshenko beams made offunctionally graded material under thermal loading", *Struct. Eng. Mech., Int. M*., **41**(6), 775-789.

Kocatürk, T. and Akbaş, Ş.D. (2013), "Thermal post-buckling analysis of functionally graded beams with temperature-dependent physical properties", *Steel Compos. Struct., Int. J*., **15**(5), 481-505.

Kocatürk, T., Şimşek, M. and Akbaş, Ş.D. (2011), "Large displacement static analysis of a cantilever Timoshenko beam composed of functionally graded material", *Sci. Eng. Compos. Mater*., **18**(1-2), 21-34.

Kolakowski, Z. and Teter, A. (2015), "Static interactive buckling of functionally graded columns with closed cross-sections subjected to axial compression", *Compos. Struct*., **123**(1), 257-262.

Li, Q. and Li, S. (2011), "Post-bucking configuration of a functionally graded material column under distributed load", *Fuhe Cailiao Xuebao*(*Acta Materiae Compositae Sinica*), **28**(3), 192-196.

Li, L.Q. and Shao, Q.H. (2014), "Non-linear analysis of a FGM cantilever beam supported on a winkler elastic foundation", *Appl. Mech. Mater*., **602**, 131-134.

Li, S.-R., Zhang, J.-H. and Zhao, Y.-G. (2006), "Thermal post-buckling of functionally graded material Timoshenko Beams", *Appl. Math. Mech.* (*English Ed.*), **26**(6), 803-810.

Marzocca, P., Fazelzadeh, S.A. and Hosseini, M. (2011), "A review of nonlinear aero-thermo-elasticity of functionally graded panels", *J. Thermal Stresses*, **34**(5-6), 536-568.

Mechab, I., Mechab, B., Benaissa, S., Serier, B. and Bouiadjra, B.B. (2016a), "Free vibration analysis of FGM nanoplate with porosities resting on Winkler Pasternak elastic foundations based on two-variable refined plate theories", *J. Brazil. Soc. Mech. Sci. Eng*., **38**(8), 2193-2211.

Mechab, B., Mechab, I., Benaissa, S., Ameri, M. and Serier, B. (2016b), "Probabilistic analysis of effect of the porosities in functionally graded material nanoplate resting on Winkler–Pasternak elastic foundations", *Appl. Math. Model*., **40**(2), 738-749.

Mohanty, S.C., Dash, R.R. and Rout, T. (2012), "Static and dynamic stability analysis of a functionally graded Timoshenko Beam", *Int. J. Struct. Stabil. Dyn*., **12**(4), 33 p.

Nguyen, D.K., Gan, B.S. and Trinh, T.H. (2014), "Geometrically nonlinear analysis of planar beam and frame structures made of functionally graded material", *Struct. Eng. Mech., Int*., **49**(6) 727-743.

Rastgo, A., Shafie, H. and Allahverdizadeh, A. (2005), "Instability of curved beams made of functionally graded material under thermal loading", *Int. J. Mech. Mater. Design*, **2**(1), 117-128.

Reddy, J.N. (2004), *An Introduction to Non-linear Finite Element Analysis*, Oxford University Press Inc., New York, NY, USA.

Şimşek, M. and Aydın, M. (2017), "Size-dependent forced vibration of an imperfect functionally graded (FG) microplate with porosities subjected to a moving load using the modified couple stress theory", *Compos. Struct.*, **160**, 408-421.

Song, X. and Li, S. (2008), "Nonlinear stability of fixed-fixed FGM arches subjected to mechanical and thermal loads", *Adv. Mater. Res.*, **33-37**, 699-706.

Sun, Y., Li, S.-R. and Batra, R.C. (2016), "Thermal buckling and post-buckling of FGM Timoshenko beams on nonlinear elastic foundation", *J. Thermal Stresses*, **39**(1) 11-26.

Trinh, T.H., Nguyen, D.K., Gan, B.S. and Alexandrov, S. (2016), "Post-buckling responses of elastoplastic FGM beams on nonlinear elastic foundation", *Struct. Eng. Mech., Int. J.*, **58**(3), 515-532.

Wattanasakulpong, N. and Ungbhakorn, V. (2014), "Linear and nonlinear vibration analysis of elastically restrained ends FGM beams with porosities", *Aerosp. Sci. Technol.*, **32**(1), 111-120.

Yan, T., Yang, J. and Kitipornchai, S. (2012), "Nonlinear dynamic response of an edge-cracked functionally graded Timoshenko beam under parametric excitation", *Nonlinear Dyn.*, **67**(1), 527-540.

Zhang, D.G. and Zhou, H.-M. (2014), "Nonlinear bending and thermal post-buckling analysis of FGM beams resting on nonlinear elastic foundations", *CMES Comput. Model. Eng.*, **100**(3) 201-222.

CC